Automatic Detection of Geospatial Objects Using Multiple Hierarchical Segmentations

H. Gökhan Akçay and Selim Aksoy, *Member, IEEE*

Abstract—**Object-based analysis of remotely sensed imagery provides valuable spatial and structural information that are complementary to pixel-based spectral information in classification. In this paper, we present novel methods for automatic object detection in high-resolution images by combining spectral information with structural information exploited using image segmentation. The proposed segmentation algorithm uses morphological operations applied to individual spectral bands using structuring elements in increasing sizes. These operations produce a set of connected components forming a hierarchy of segments for each band. A generic algorithm is designed to select meaningful segments that maximize a measure consisting of spectral homogeneity and neighborhood connectivity. Given the observation that different structures appear more clearly at different scales in different spectral bands, we describe a new algorithm for unsupervised grouping of candidate segments belonging to multiple hierarchical segmentations to find coherent sets of segments that correspond to actual objects. The segments are modeled using their spectral and textural content, and the grouping problem is solved using the probabilistic Latent Semantic Analysis algorithm that builds object models by learning the object-conditional probability distributions. Automatic labeling of a segment is done by computing the similarity of its feature distribution to the distribution of the learned object models using Kullback-Leibler divergence. The performances of the unsupervised segmentation and object detection algorithms are evaluated qualitatively and quantitatively using three different data sets with comparative experiments, and the results show that the proposed methods are able to automatically detect, group and label segments belonging to the same object classes.**

Index Terms—**Image segmentation, unsupervised object detection, mathematical morphology, hierarchical segmentation, object-based analysis.**

I. Introduction

Due to the constantly increasing coverage and availability of very high-resolution remotely sensed data, automatic content extraction, object detection and classification for urban applications have continued to be important research problems. There is an extensive literature on classification of remotely sensed imagery where pixel level processing has been the common choice for remote sensing image analysis systems. These systems use a broad range of features including multi- or hyper-spectral information, texture features, edge detection, as well as linear or nonlinear transformations of these features. Such features are used with a wide range of classifiers including probabilistic methods employing maximum likelihood or Bayesian estimation techniques, neural networks, decision trees, support vector machines and genetic algorithms for applications like land cover/use classification.

Despite the high success rates that have been published in the literature using limited ground truth data, visual inspection of the results shows that most of the urban structures still cannot be delineated as accurately as expected especially in high-resolution images. For example, Figure 1(a) shows the false color representation of a hyper-spectral image of Pavia, Italy. The classification map shown in Figure 1(c) is obtained using features extracted with PCA and Gabor texture filters with a quadratic Gaussian classifier [1]. Similarly, Figure 1(d) shows the map obtained using discriminant analysis feature extraction (DAFE) and a similar classifier [2]. Even though the success rates obtained as 93.97% and 97.2%, respectively, according to the reference map shown in Figure 1(b) can be considered quite high, none of the boundaries of the buildings, roads and shadows on the left half of the image is explicit and no structure can be seen in the results. In other words, the limitations of pixel-based classification evaluated using limited pixel-based ground truth are not necessarily reflected in the numerical accuracy. Therefore, this shows that there is still much work to be done, and more advanced classification methods must be designed for practically acceptable results.

We believe that, in addition to pixel-based spectral data, spatial and structural information should also be used for more intuitive and accurate classification. Common ways of incorporating spatial information into classification involve the use of textural, morphological and object-based features. Features extracted using co-occurrence matrices, Gabor wavelets [3], morphological profiles [4], and Markov random fields [5] have been widely used in the literature to model spatial information in neighborhoods of pixels. However, problems such as scale selection and the detailed content of very high-resolution imagery make the applicability of traditional fixed window-based methods difficult for such data sets.

Another powerful method for exploiting structural information is to perform region-based classification rather than classifying individual pixels. This is also referred to as object-oriented classification in the remote sensing literature. For example, Bruzzone and Carlin [6] performed classification using the spatial context of each pixel according to a hierarchical multi-level representation of the scene. In a similar approach [7], we obtained a wavelet-based multi-resolution representation, segmented images at each resolution, and used region-based spectral, textural and shape features for classification. In [8], Katartzis *et al.* also modeled spatial information by segmenting images into regions and classifying these regions

Manuscript received November 3, 2007; revised December 19, 2007. This work was supported in part by the TUBITAK CAREER Grant 104E074 and European Commission Sixth Framework Programme Marie Curie International Reintegration Grant MIRG-CT-2005-017504.

The authors are with Department of Computer Engineering, Bilkent University, Ankara, 06800, Turkey. Email: {akcay,saksoy}@cs.bilkent.edu.tr.

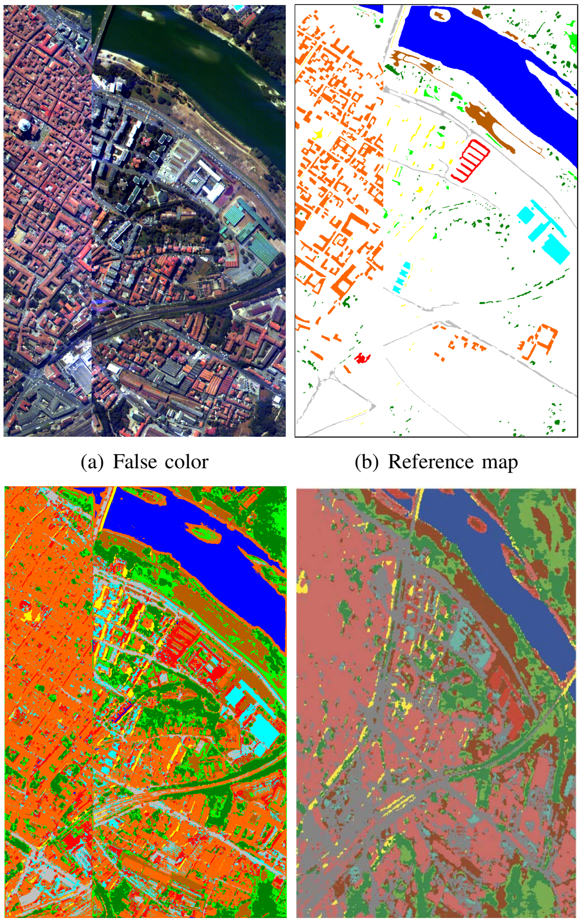

(a) False color

(b) Reference map

(c) Classification using PCA and Gabor features

(d) Classification using DAFE features

Fig. 1. Example classification results using a pixel-based quadratic Gaussian classifier with PCA and Gabor features (c) and DAFE features (d). The classification maps for (c) and (d) are taken from [1] and [2], respectively.

using a Markovian model, defined on the hierarchy of a multi-scale region adjacency graph. In another study [9], Soh *et al.* presented a system for sea ice image classification which also segmented the images, generated descriptors for the segments and then used expert system rules to classify the images.

Many popular segmentation algorithms in the computer vision literature assume that images have a moderate number of objects with relatively homogeneous features, and cannot be directly applied to high-resolution remote sensing images that contain a large number of complex structures. Furthermore, another popular approach of edge-based segmentation is hard for such images because of the large amount of details. Moreover, watershed-based techniques are also not very useful because they often produce oversegmented results mostly because of irrelevant local extrema in images. A common approach is to apply smoothing filters to suppress these extrema but lots of details in high-resolution images may be lost because spatial support of these details are usually small. Therefore, most of the segmentation work in the remote sensing literature have been based on merging neighboring pixels according to user-defined thresholds on their spectral similarity. Alternatively, proximity filtering and morphological operations can also be used as post-processing techniques to pixel-based classification results for segmenting regions [10].

In a related work, Pesaresi and Benediktsson [4] successfully applied opening and closing operations with increasing structuring element sizes to an image to generate morphological profiles for all pixels, and assigned a segment label to each pixel using the structuring element size corresponding to the largest derivative of these profiles. Even though morphological profiles are sensitive to different pixel neighborhoods, the segmentation decision is performed by evaluating pixels individually without considering the neighborhood information, and the assumption that all pixels in a structure have only one significant derivative maximum occurring at the same structuring element size often does not hold for very high-resolution images. Scale selection is also a very important problem in multi-scale/hierarchical segmentation techniques. For example, Tilton [11] developed a hierarchical segmentation algorithm that combined spectral clustering with iterative region growing in which segments at coarser levels of detail were obtained by merging segments at finer levels of detail. The multi-resolution segmentation implementation offered by the eCognition software also consists of bottom-up region merging where each pixel is initially considered as a separate object and pairs of image objects are iteratively merged to form larger segments [12]. The main problems associated with both of these approaches are that the resulting segmentations depend on the thresholds used with local homogeneity criteria, and manual interpretation of the hierarchy is needed because different objects may appear at different scales.

Our main contributions in this paper are twofold: we present a new segmentation algorithm for exploiting structural information, and propose a novel method that uses the resulting regions for unsupervised object detection. Our first contribution, the segmentation algorithm, uses the neighborhood and spectral information as well as the morphological information. First, morphological opening and closing operations are applied to individual spectral bands using structuring elements in increasing sizes to generate morphological profiles. These operations produce a set of connected components forming a hierarchy of segments for each band. Then, unlike [4] where only the scale with the maximum change in the profile is considered, each component at different levels of the hierarchy is evaluated as a candidate for meaningful structures using a measure that consists of two factors: spectral homogeneity, which is calculated in terms of variances of spectral features, and neighborhood connectivity, which is calculated using sizes of connected components. A novel two-pass algorithm is designed to select the segments that jointly optimize this combined measure and find the meaningful segments in a completely unsupervised process. The proposed selection algorithm is generic in the sense that other criteria for homogeneity and connectivity can also be directly incorporated.

An important observation is that different structures appear more clearly in different bands. For example, buildings can be detected accurately in one band but roads, trees, fields and paths can be detected accurately in other bands. With a similar observation, Benediktsson *et al.* [2] appended the morphological profiles that were independently extracted from multiple principal components into a single high-dimensional feature vector, performed linear feature reduction, and classified the pixels using neural networks.

In this paper, as our second main contribution, we propose a novel unsupervised method for automatic detection of objects from multiple hierarchical segmentations and the corresponding candidates for meaningful structures from individual bands. The goal is to find coherent groups of segments that correspond to actual objects. Considering multiple objects/structures of interest, this setting can also be seen as a grouping problem within the space of a large number of candidate segments obtained from multiple hierarchical segmentations. To solve the grouping problem, we use the probabilistic Latent Semantic Analysis (PLSA) [13] technique by formulating a graphical model for the joint probability of the segments and their features in terms of the probability of observing a feature given an object and the probability of an object given the segment. The parameters of this graphical model are learned using the Expectation-Maximization algorithm. Then, for a particular segment, the set of probabilities of objects/structures given this segment can be used to assign an object label to this segment. The performances of the unsupervised segmentation and automatic object detection algorithms are evaluated qualitatively and quantitatively using three different data sets with comparative experiments.

The rest of the paper is organized as follows. The data sets and the features used for both segmentation and object detection are introduced in Section II. The segmentation algorithm for the extraction of candidate segments from individual bands in an image is described in Section III. The algorithm for grouping segments for object detection is presented in Section IV. Experiments are discussed in Section V and conclusions are given in Section VI.

II. Feature Extraction

We illustrate the proposed algorithms using three data sets:

1) *DC Mall*: HYDICE image with $1,280 \times 307$ pixels, 3 m spatial resolution, and 191 spectral bands corresponding to an airborne data flightline over the Washington DC Mall area. The false color image is given in Figure 2(a).
2) *Pavia*: ROSIS data with $1,096 \times 715$ pixels, 2.6 m spatial resolution, and 102 spectral bands corresponding to the city center in Pavia, Italy. The false color image is given in Figure 3(a).
3) *Ankara*: IKONOS data with 500×500 pixels and 1 m spatial resolution pan-sharpened RGB bands corresponding to part of a university campus in downtown Ankara. The color image is given in Figure 19(a).

Since morphological operations have traditionally been defined for single band binary or gray scale images, we applied principal components analysis (PCA) to summarize the hyperspectral data as the PCA bands provide the optimal representation in the least-squares sense [14]. The resulting three bands corresponding to the top principal components representing the 99% variance of the whole data are shown in Figures 2 and 3 for the *DC Mall* and *Pavia* data sets, respectively. Original RGB bands were used for the *Ankara* data set.

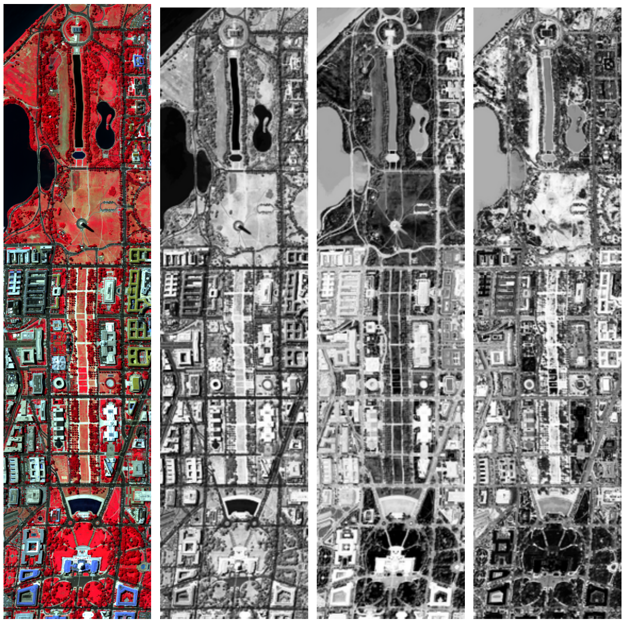

(a) False color (b) 1st band (c) 2nd band (d) 3rd band

Fig. 2. False color image (generated using the bands 63, 52 and 36) and the first three PCA bands of the *DC Mall* data set.

In addition to the PCA bands that give the best representation, we also applied linear discriminant analysis (LDA) that projects the data onto a new set of bases that best separate the classes in the least-squares sense [14]. 6 bands for the *DC Mall* and 8 bands for the *Pavia* data sets were extracted using the pixel level 7 class and 9 class ground truth available for these data sets, respectively. Finally, we extracted Gabor texture features [3] using kernels at 2 scales and 4 orientations resulting in an additional feature vector of length 8 for each pixel for a given band. The resulting PCA bands are used for image segmentation as the best representation for the spectral data in Section III, and the LDA and Gabor bands are used as alternative features, in addition to the PCA bands, for object detection in Section IV.

III. Image Segmentation

The proposed segmentation algorithm combines spectral information from the original data with structural information extracted through morphological operations. These two complementary types of information are incorporated into a hierarchical structure, and a generic iterative algorithm is used to extract meaningful segments from this hierarchy by simultaneously optimizing spectral homogeneity and neighborhood connectivity. Considering the fact that different structures may appear more clearly in different bands, we analyze each band separately. The following sections describe the details of the algorithm. Parts of this section were presented in [15].

A. Morphological Profiles

We use mathematical morphology to exploit structural information. In particular, morphological opening and closing operations are used to model structural characteristics of pixel neighborhoods. These operations are known to isolate

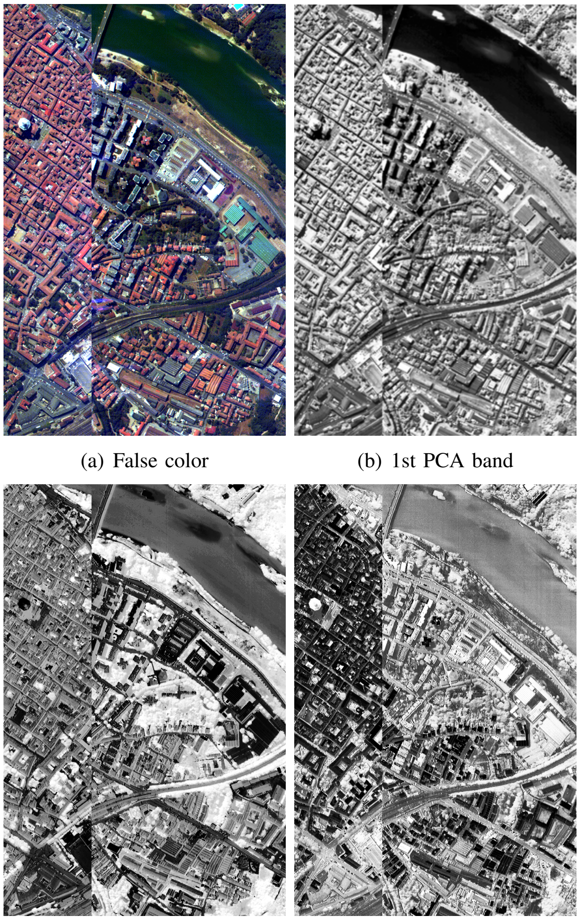
(a) False color (b) 1st PCA band

(c) 2nd PCA band (d) 3rd PCA band

Fig. 3. False color image (generated using the bands 68, 30 and 2) and the first three PCA bands of the *Pavia* data set. (A missing vertical section in the middle was removed.)

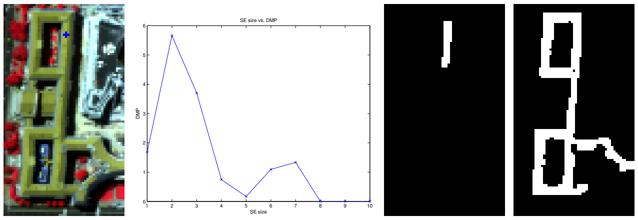

(a) An example pixel (b) DMP of the pixel (c) Segment for SE size 2 (d) Segment for SE size 3

Fig. 4. The greatest value in the DMP of the pixel marked with a blue + in (a) is obtained for SE size 2 (derivative of the opening profile is shown in (b)). (c) shows the segment that we would obtain if we label the pixels with the SE size corresponding to the greatest DMP. The segment in (d) that occurs with SE size 3 is more preferable as a complete structure but it does not correspond to the scale of the greatest DMP for all pixels inside the segment.

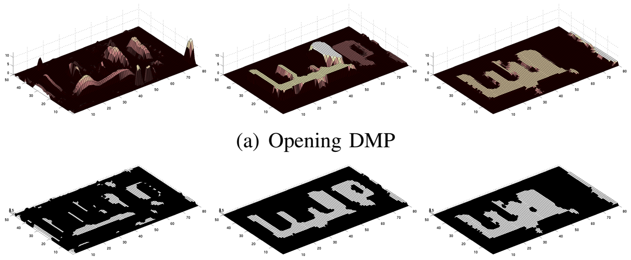
(a) Opening DMP

(b) Thresholding at DMP > 0

Fig. 5. (a) Example DMP at three scales. (b) The pixels whose DMP values are greater than 0. Each connected component at each scale is a candidate segment for the final segmentation.

structures that are brighter and darker than their surroundings, respectively. Contrary to opening (respectively, closing), opening by reconstruction (respectively, closing by reconstruction) preserves the shape of the structures that are not removed by erosion (respectively, dilation). In other words, image structures that the structuring element (SE) cannot be contained are removed while others remain.

The opening and closing by reconstruction operations are applied using increasing SE sizes to generate multi-scale characteristics called morphological profiles. The derivative of the morphological profile (DMP) [4] is defined as a vector where the measure of the slope of the opening-closing profile is stored for every step of an increasing SE series. Pesaresi and Benediktsson [4] used the structural information encoded in the DMP for segmenting remote sensing images. They defined an image segment as a set of connected pixels showing the greatest value of the DMP for the same SE size. That is, the segment label of each pixel is assigned according to the scale corresponding to the largest derivative of its profile. Their scheme works well in images with moderate resolution where the structures in the image are mostly flat so that all pixels in a structure have only one derivative maximum. A drawback of this scheme is that neighborhood information is not used while assigning segment labels to pixels. This often results in lots of small noisy segments in very high-resolution images with non-flat structures where the scale with the largest value of the DMP may not correspond to the true structure (see Figure 4 for an illustration). In our approach, we do not consider pixels alone while assigning segment labels. Instead, we also take into account the behavior of the neighbors of the pixels.

B. Hierarchical Segment Extraction

In our segmentation approach, our aim is to determine the segments by applying opening and closing by reconstruction operations. We assume that pixels with a positive DMP value at a particular SE size face a change with respect to their neighborhoods at that scale. As opposed to [4] where only the scale corresponding to the greatest DMP is used, the main idea is that a neighboring group of pixels that have a similar change for any particular SE size is a candidate segment for the final segmentation. These groups can be found by applying connected components analysis to the DMP at each scale (see Figure 5 for an illustration).

Considering the fact that different structures have different sizes, we apply opening and closing by reconstruction using SEs in increasing sizes from 1 to m (radius of disk). However, a connected component appearing for a small SE size may be appearing because of heterogeneity and geometrical complexity of the scenes as well as other external effects such as shadows producing texture effects in images and resulting in structures that can be one to two pixels wide [4]. In this case, there is most probably a larger connected component

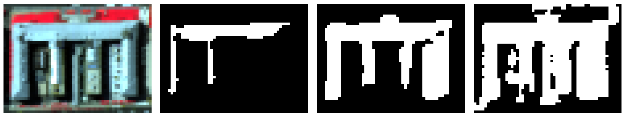

(a) False color image (b) A small connected component that is part of (c) (c) The preferred connected component (d) A large component where (c) started merging with others

Fig. 6. Example connected components for a building structure. These components appear for SE sizes 3, 5 and 6, respectively, in the derivative of the opening profile of the 2nd PCA band.

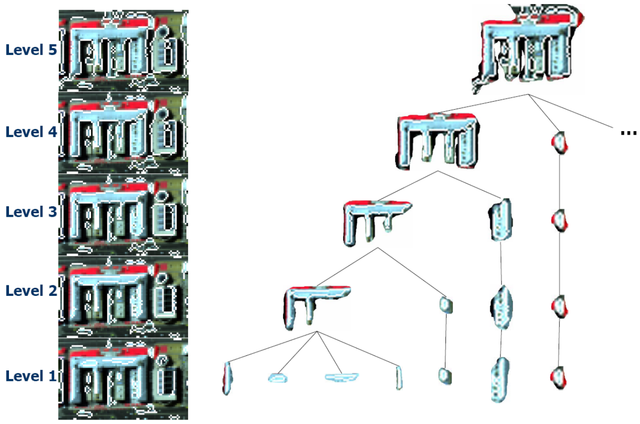

Fig. 7. An example tree where each candidate segment is a node.

appearing at the scale of a larger SE and to which the pixels of those noise components belong. On the other hand, a connected component that corresponds to a true structure in the final segmentation may also appear as part of another component at larger SE sizes. The reason is that a meaningful connected component may start merging with its surroundings and other connected components after the SE size in which it appears is reached. Figure 6 illustrates these cases.

For each opening and closing profile, through increasing SE sizes from 1 to m, each morphological operation reveals connected components that are contained within each other in a hierarchical manner where a pixel may be assigned to more than one connected component appearing at different SE sizes as in Figure 6. We treat each component as a candidate meaningful segment. Using these segments, a tree is constructed where each connected component is a node and there is an edge between two nodes corresponding to two consecutive scales if one node is contained within the other. Leaf nodes represent the components that appear for SE size 1. Root nodes represent the components that exist for SE size m. Figure 7 shows a part of an example tree constructed by candidate meaningful segments appearing in five levels. Since we use a finite number of SE sizes, there may be more than one root node. In this case, there will be more than one tree and the algorithms described in the next section are run on each tree separately.

C. Segment Selection

After forming a tree for each opening and closing profile, our aim is to search for the most meaningful connected components among those appearing at different scales in the segmentation hierarchy. With a similar motivation in [11], Tilton analyzed hierarchical image segmentations and selected the meaningful segments manually. Then, Plaza and Tilton [16] investigated how different spectral, spatial and joint spectral/spatial features of segments change from one level to another in a segmentation hierarchy with the goal of automating the selection process in the future. Alternatively, Klaric *et al.* [17] thresholded the DMP to obtain candidate objects, and applied heuristics such as thresholds on the aspect ratio of the bounding box to accept a candidate as a building object. In this paper, each node in the tree is treated as a candidate segment in the final segmentation, and selection is done automatically as described below.

Ideally, we expect a meaningful segment to be spectrally as homogeneous as possible. However, in the extreme case, a single pixel is the most homogeneous. Hence, we also want a segment to be as large as possible. In general, a segment stays almost the same (both in spectral homogeneity and size) for some number of SEs, and then faces a large change at a particular scale either because it merges with its surroundings to make a new structure or because it is completely lost. Consequently, the size we are interested in corresponds to the scale right before this change. In other words, if the nodes on a path in the tree stay homogeneous until some node n, and then the homogeneity is lost in the next level, we say that n corresponds to a meaningful segment in the hierarchy.

With this motivation, to check the meaningfulness of a node, we define a measure consisting of two factors: spectral homogeneity, which is calculated in terms of variances of spectral features, and neighborhood connectivity, which is calculated using sizes of connected components. Then, starting from the leaf nodes (level 1) up to the root node (level m), we compute this measure at each node and select a node as a meaningful segment if it is highly homogeneous and large enough node on its path in the hierarchy (a path corresponds to the set of nodes from a leaf to the root).

In order to calculate the homogeneity factor in a node, we use the fact that pixels in a correct structure should have not only similar morphological profiles, but also similar spectral features. Thus, we calculate the homogeneity of a node as the standard deviation of the spectral information of the pixels in the corresponding segment. The spectral information for the *DC Mall* and *Pavia* data sets consist of the PCA bands whereas the RGB bands are used for the *Ankara* data set. The PCA components are used instead of the full hyper-spectral data because they achieve dimensionality reduction and provide the best summarization of spectral data in the least-squares sense. The LDA bands are not used because their computation requires labeled data but we want the segmentation step to be fully unsupervised. The rest of the algorithm is generic; thus, is independent from which features are used to compute spectral homogeneity.

While examining a node from the leaf up to the root in terms of homogeneity, we do not use the standard deviation of the node directly. Instead, we consider the difference of the standard deviation of that node and its parent. What we expect is a sudden increase in the standard deviation. When the standard deviation does not change much, it usually means that small sets of pixels are added to the segment or some noise pixels are cleaned. When there is a large change, it means that the structure merged with a larger structure or it merged with other irrelevant pixels disturbing the homogeneity in the node. Hence, the difference of the standard deviation in the node's parent and the standard deviation in the node should be maximized while selecting the most meaningful nodes.

The computation of the standard deviation of multi-spectral data of a node is done by projecting these data onto a 1-dimensional representation [18]. Let the number of spectral bands be d. The basis used for the 1-dimensional representation is selected as the vector connecting the mean of the original d-dimensional data for the pixels of the current node and the mean of the data for its parent. The projection of the d-dimensional data onto this vector, that can be considered to separate the nodes in the spectral space, is computed using inner products, and the standard deviation of the resulting 1-dimensional data is computed for each node. This formulation exploits the multivariate information contained in the multi-spectral bands while computing the standard deviation. We also tested using the average of the standard deviations computed from individual bands, but there was no visual difference in the results compared to the ones given in the paper.

As discussed above, using only the spectral homogeneity factor will favor small structures. To overcome this problem, the number of pixels in the segment corresponding to the node is introduced as another factor to create a trade-off. As a result, the goodness measure M for a node n is defined as

$$M(n) = D(n, parent(n)) \times C(n) \tag{1}$$

where the first term is the standard deviation difference between the node's parent and itself, and the second term is the number of pixels in the node. The node that is relatively spectrally homogeneous and large enough will maximize this measure and will be selected as a meaningful segment. Other linear and nonlinear combinations of homogeneity and scale can be incorporated for calculating the goodness measure. However, we use the simplest combination in (1) to avoid introducing new parameters.

Given the value of the goodness measure for each node, we find the most meaningful segments as follows. Suppose $\mathcal{T} = (\mathcal{N}, \mathcal{E})$ is the tree with $\mathcal{N}$ as the set of nodes and $\mathcal{E}$ as the set of edges. The leaf nodes are in level 1 and the root node is in level m. Let $\mathcal{P}$ denote the set of all paths from the leaves to the root, $M(n)$ denote the measure at node n, and $descendant(n)$ denote descendant nodes of node n. We select $\mathcal{N}^* \subseteq \mathcal{N}$ as the final segmentation such that

1) $\forall a \in \mathcal{N}^*, \forall b \in descendant(a),$
   $M(a) \geq M(b),$
2) $\forall a \in \mathcal{N} \setminus \mathcal{N}^*,$
   $\exists b \in descendant(a) : M(a) < M(b),$
3) $\forall a, b \in \mathcal{N}^*,$
   $\forall p \in \mathcal{P} : a \in p \rightarrow b \notin p,$
   $\forall p \in \mathcal{P} : b \in p \rightarrow a \notin p,$
4) $\forall p \in \mathcal{P},$
   $\exists a \in p : a \in \mathcal{N}^*.$

The first condition requires that any node in $\mathcal{N}^*$ must have a measure greater than all of its descendants. The second condition requires that no node in $\mathcal{N} \setminus \mathcal{N}^*$ has a measure greater than all of its descendants. The third condition requires that any two nodes in $\mathcal{N}^*$ cannot be on the same path (i.e., the corresponding segments cannot overlap in the hierarchical segmentation). The fourth condition requires that every path must include a node that is in $\mathcal{N}^*$.

We use a two-pass algorithm for selecting the most meaningful nodes ($\mathcal{N}^*$) in the tree. The bottom-up (first) pass aims to find the nodes whose measure is greater than all of its descendants (condition 1). The algorithm first marks all nodes in level 1. Then, starting from level 2 up to the root level, it checks whether each node in each level has a measure greater than or equal to those of all of its children. The greatest measure, seen so far in each path, is propagated to upper levels so that it is enough to check only the immediate children, rather than all descendants, in order to find whether a node's measure is greater than or equal to all of its descendants'.

After the bottom-up pass marks all such nodes, the top-down (second) pass seeks to select the nodes satisfying, as well, the remaining conditions (2, 3 and 4). It starts by marking all nodes as *selected* in the root level if they are marked by the bottom-up pass. Then, in each level until the leaf level, the algorithm checks for each node whether it is marked in the bottom-up pass while none of its ancestors is marked. If this condition is satisfied, it marks the node as *selected*. Finally, the algorithm selects the nodes that are marked as *selected* in each level as meaningful segments. The pseudocode for the selection algorithm is shown in Algorithms 1–3.

An example run of these algorithms is illustrated using a sample tree where the nodes are labeled as i_j with i denoting the node's level and j denoting the number of the node from left to right in that level. A value for the goodness measure is given in parenthesis for each node. Figures 8 and 9 show the marked nodes in each step of the Bottom-Up and the Top-Down algorithms, respectively. During the Bottom-Up algorithm, each node 1_j $(1 \leq j \leq 8)$ is marked in the beginning. Then, as we move upwards, nodes $2\_1, 2\_2, 2\_3, 2\_5$ in level 2, and nodes 3_1 and 3_2 in level 3 are marked since the measure of each of them is greater than or equal to those of all of its descendants. Then, we run the Top-Down algorithm and mark nodes $3\_1, 3\_2, 2\_5$ and 1_5, satisfying the four conditions defined above, as *selected*.

After selecting the most meaningful connected components in each opening and closing tree separately, the next step is to

Algorithm 1 Segment Selection Algorithm

```
Run Bottom-Up algorithm
Run Top-Down algorithm
for each level $l = 1$ to $m$ do
    for each node $n$ in level $l$ do
        select $n$ as a meaningful segment if it is marked as selected
    end for
end for
```

Algorithm 2 Bottom-Up Algorithm

```
Mark all nodes in level 1
for each level $l = 2$ to $m$ do
  for each node $n$ in level $l$ do
    if $M(n) \geq \max\{M(a)|a \in children(n)\}$ then
      mark $n$
    else
      $M(n) = \max\{M(a)|a \in children(n)\}$
      leave $n$ unmarked
    end if
  end for
end for
```

Algorithm 3 Top-Down Algorithm

```
Mark all nodes in level $m$ as selected if they are already marked in Bottom-Up
for each level $l = m - 1$ to 1 do
  for each node $n$ in level $l$ do
    if $parent(n)$ is marked as selected or parent-selected then
      mark $n$ as parent-selected
    else
      if $parent(n)$ is not marked in Top-Down and $n$ is not marked in Bottom-Up then
        leave $n$ unmarked
      else
        mark $n$ as selected
      end if
    end if
  end for
end for
```

integrate the resulting connected components. A problem may occur when two connected components, one being selected from the opening tree and the other being selected from the closing tree, intersect. In this case, the intersecting part is assigned to the connected component whose goodness measure is greater.

D. Evaluation of Segmentation

We applied the proposed hierarchical segmentation algorithm to all three data sets described in Section II. Disk structuring elements with radii from 3 to 15 were used for both opening and closing profiles constructed for each spectral band (3 PCA bands for *DC Mall* and *Pavia*, 3 RGB bands for *Ankara*). The tree structure was constructed for each band separately, and the segments were selected from each tree independently. The same bands were also segmented using the Pesaresi-Benediktsson algorithm [4] that defines an image segment as a set of connected pixels showing the greatest value of the derivative morphological profile for the same structuring element size, and the watershed segmentation [19] that uses the gradient of an image as input after suppressing small local extrema to avoid severe oversegmentation. The same parameters were used for all data sets for a given algorithm.

Table I shows the total number of segments obtained using all three algorithms. Figures 10, 11 and 12 show example segmentations for the *DC Mall*, *Pavia* and *Ankara* data sets, respectively. We present the zoomed versions of the results for several example areas to better illustrate the details for high-resolution imagery and for clarity of the presentation on paper. Since there is no detailed object level GIS vector data available, only qualitative evaluation is done for segmentation. The results show that our segmentation algorithm is able to detect structures in the image that are more precise and more meaningful than the structures detected by the compared approaches. The oversegmentation produced by the Pesaresi-

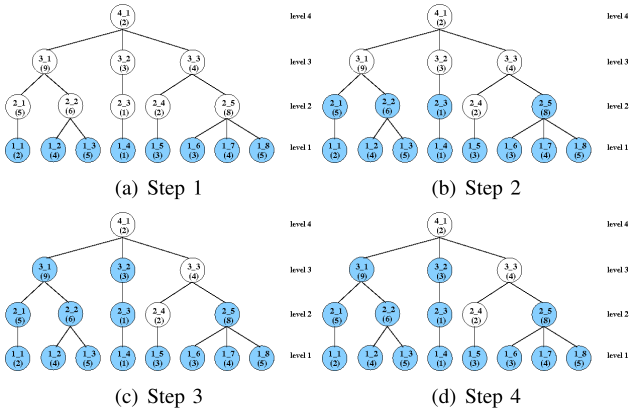

(a) Step 1 (b) Step 2

(c) Step 3 (d) Step 4

Fig. 8. An example run of the Bottom-Up algorithm on a sample tree. Beginning from the leaves until the root, the nodes whose measures are greater than all of the descendants (satisfying condition 1) are colored with blue in each step.

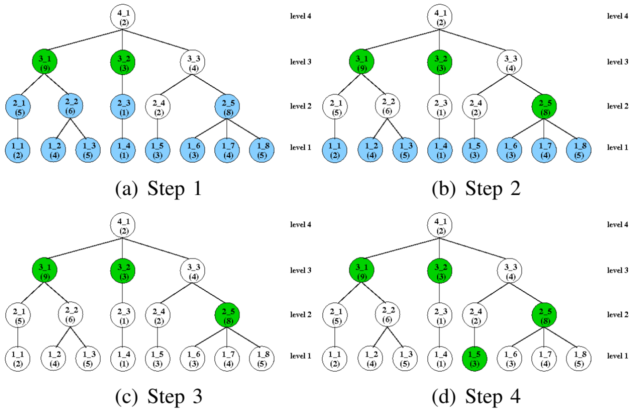

(a) Step 1 (b) Step 2

(c) Step 3 (d) Step 4

Fig. 9. An example run of the Top-Down algorithm on the tree in Figure 8(d). Beginning from the root until the leaves, the nodes marked in the Bottom-Up algorithm which satisfy, as well, the remaining conditions (2, 3 and 4) are marked with green in each step. When the algorithm ends, the green nodes are selected as the most meaningful nodes in the tree.

TABLE I

TOTAL NUMBER OF SEGMENTS OBTAINED USING DIFFERENT SEGMENTATION ALGORITHMS FOR INDIVIDUAL BANDS. HS: PROPOSED HIERARCHICAL SEGMENTATION ALGORITHM, PB: PESARESI-BENEDIKTSSON ALGORITHM, WS: WATERSHED SEGMENTATION.

	DC Mall			*Pavia*			*Ankara*		
	PCA1	PCA2	PCA3	PCA1	PCA2	PCA3	Red	Green	Blue
HS	647	710	713	1420	1432	1255	341	353	359
PB	30240	28097	280206	65296	63394	61965	16258	18057	15840
WS	14640	13653	1962	21817	14143	6537	7009	6335	4666

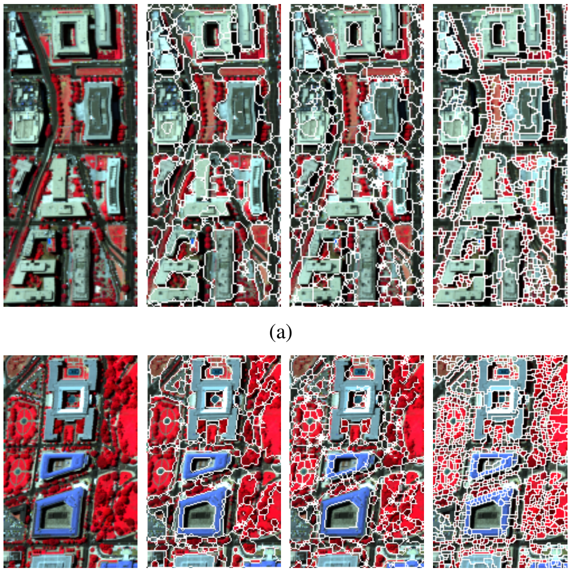

(a)

(b)

Fig. 10. Example segmentation results for the *DC Mall* data set. From left to right: false color, result of the proposed approach, result of Pesaresi-Benediktsson, result of watershed segmentation.

Benediktsson algorithm is because the segment label assignment is done for each pixel individually by only considering the greatest value in its DMP. Thus, noisy pixels that are different from their neighborhoods may produce small segments because they may have large values occurring at scales corresponding to small SE sizes. Similarly, even though a prefiltering to suppress the small local extrema of the gradient is applied, the watershed segmentation algorithm still produces oversegmentation as commonly observed in the literature. However, our algorithm considers both the morphological characteristics encoded in the DMP and the spectral homogeneity measured in terms of the standard deviation within contiguous groups of pixels. It also considers the consistency of these values within neighboring pixels forming large connected components. As a result, the combined measure that uses both spectral and structural information is both robust to noise and consistent within detailed structures in high-resolution images. In all of the examples, our algorithm is able to extract many meaningful structures as whole segments.

Note that it is possible to improve some of the segments by tuning the parameters of the Pesaresi-Benediktsson algorithm (e.g., specifying different set of scales) and the watershed segmentation algorithm (e.g., threshold for eliminating small local extrema). (Same parameters were used for all algorithms for all data sets in the experiments.) However, we observed that different parameters needed to be selected manually for different bands of different data sets, and the parameters that performed well for one band of a data set could give very bad results for other bands and other data sets. On the other hand, the proposed segment extraction and segment selection algorithms are free from parameters (except the number of scales, m, used to construct the range of structuring element sizes with fixed unit increments for the morphological profile for segment extraction), and can automatically select the meaningful segments at different scales and sizes in the hierarchy for different spectral bands and different data sets in a completely unsupervised process without any need for parameter tuning.

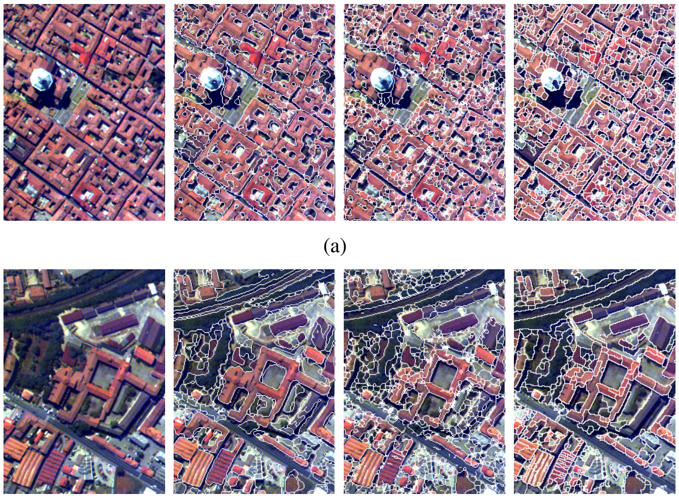

(a)

(b)

Fig. 11. Example segmentation results for the *Pavia* data set. From left to right: false color, result of the proposed approach, result of Pesaresi-Benediktsson, result of watershed segmentation.

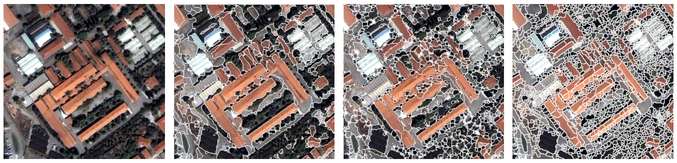

Fig. 12. Example segmentation results for the *Ankara* data set. From left to right: RGB color, result of the proposed approach, result of Pesaresi-Benediktsson, result of watershed segmentation.

Another important observation is that different structures are extracted more clearly in different spectral bands. In particular, buildings can be detected accurately in one band but roads, trees, fields, paths and shadows can be detected accurately in other bands. For example, the structures in both Figures 10(a) and 10(b) are found in the second PCA band of the *DC Mall* data set. On the other hand, the structures in both Figures 11(a) and 11(b) are found in the third PCA band of the *Pavia* data set. Figure 13 shows the extracted segments in different PCA bands of the *DC Mall* data set. The reason that a particular structure being extracted better in a particular band is that the pixels belonging to that structure are found lighter or darker than their surroundings on that band. This motivates the next step on automatically integrating the results from individual bands as a final segmentation with detected objects in an image.

IV. Object Detection

In Section III, we described a method that used the neighborhood and spectral information as well as the morphological information for segmentation. In this section, we present an unsupervised algorithm for automatic selection of segments from multiple segmentations and spectral bands. (Parts of this

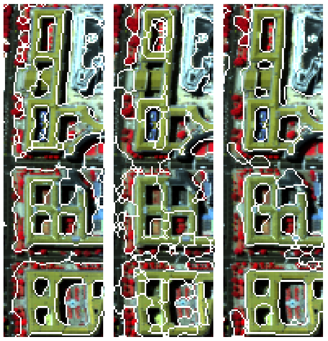

Fig. 13. Example segmentation results for different PCA bands of the *DC Mall* data set. The left, middle and right images show the segments extracted in the first, second and third PCA bands where the roads/shadows, trees and buildings are detected more clearly, respectively.

section were presented in [20].) The input to the algorithm is a set of hierarchical segmentations corresponding to different spectral bands. The goal is to find coherent groups of segments that correspond to meaningful structures. The assumption here is that, for a particular structure (e.g., building), the "good" segments (i.e., the ones containing a building) will all have similar features whereas the "bad" segments (i.e., the ones containing multiple objects or corresponding to overlapping partial object boundaries) will be described by a random mixture of features. Therefore, considering multiple objects/structures of interest, this selection process can also be seen as a grouping problem within the space of a large number of candidate segments obtained from multiple hierarchical segmentations. The resulting groups correspond to different types of objects in the image.

A. Modeling Segments

The grouping algorithm consists of three steps: extracting segment features, grouping segments, detecting objects. In the first step, each segment is modeled using the statistical summary of its pixel content. First, all pixels in the image are clustered by applying the k-means algorithm in a feature domain. This corresponds to quantization of the feature values. Then, a histogram is constructed for each segment to approximate the distribution of these quantized values belonging to the pixels in that segment as shown in Figure 14. This histogram is used to represent the segment in the rest of the algorithm. Alternative representations include using the mean or the covariance of the feature values of the pixels within a segment. However, the mean is often not sufficient to distinguish complex objects, and the covariance estimation can have singularity problems for small sample sizes. The histogram model provides a trade-off that contains more information than the mean while being easier to estimate than the covariance. Furthermore, the segment selection algorithm in Section III-C uses a goodness measure that selects the segments that are large enough, so that the histograms can be reliably estimated. Note that the object detection algorithm is generic in the sense that any discrete model of the segment's content can also be used by the grouping algorithm in the next section.

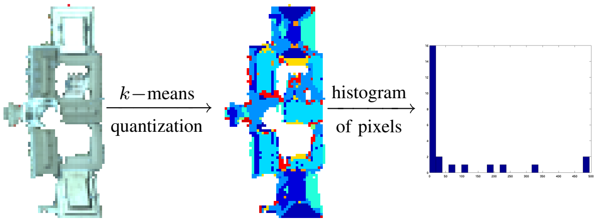

Fig. 14. Each segment is modeled using the statistical summary of its pixel content. In the experiments, these summaries are obtained by quantizing the feature values using the k-means algorithm and representing the distribution of these quantized values in a histogram.

B. Grouping Segments

In this work, we use the probabilistic Latent Semantic Analysis (PLSA) algorithm [13] to solve the grouping problem. PLSA was originally developed for statistical text analysis to discover topics in a collection of documents that are represented using the frequencies of words from a vocabulary. In our case, the documents correspond to image segments, the word frequencies correspond to histograms of pixel level features, and the topics to be discovered correspond to the set of objects/structures of interest in the image. Russell *et al.* [21] used a different graphical model in a similar setting where multiple segmentations of natural images were obtained using the normalized cut algorithm by changing its parameters, and instances of segments corresponding to objects such as cars, bicycles, faces, sky, etc., were successfully grouped and retrieved from a large set of images.

The PLSA technique uses a graphical model for the joint probability of the segments and their features in terms of the probability of observing a feature given an object and the probability of an object given the segment. Suppose there are N segments (documents) having content coming from a distribution (vocabulary) with M discrete pixel feature values (words). The collection of segments is summarized in an N-by-M co-occurrence table n where $n(s_i, x_j)$ stores the number of occurrences of feature value x_j in segment s_i. In addition, there is a latent object type (topic) variable t_k associated with each observation, an observation being the occurrence of a feature in a particular segment.

The graphical model used by PLSA to model the joint probability $P(x_j, s_i, t_k)$ is shown in Figure 15. The generative model $P(s_i, x_j) = P(s_i)P(x_j|s_i)$ for feature content of segments can be computed using the conditional probability

$$P(x_j|s_i) = \sum_{k=1}^{K} P(x_j|t_k)P(t_k|s_i) \tag{2}$$

where $P(x_j|t_k)$ denotes the object-conditional probability of feature x_j occurring in object t_k, $P(t_k|s_i)$ denotes the probability of object t_k observed in segment s_i, and K is the number of object types. Then, the object specific feature distribution $P(x_j|t_k)$ and the segment specific feature distribution $P(x_j|s_i)$ can be used to determine similarities between object types and segments (explained in the next section).

In PLSA, the goal is to identify the probabilities $P(x_j|t_k)$ and $P(t_k|s_i)$. These probabilities are learned using the Expectation-Maximization (EM) algorithm [13]. In the E-step,

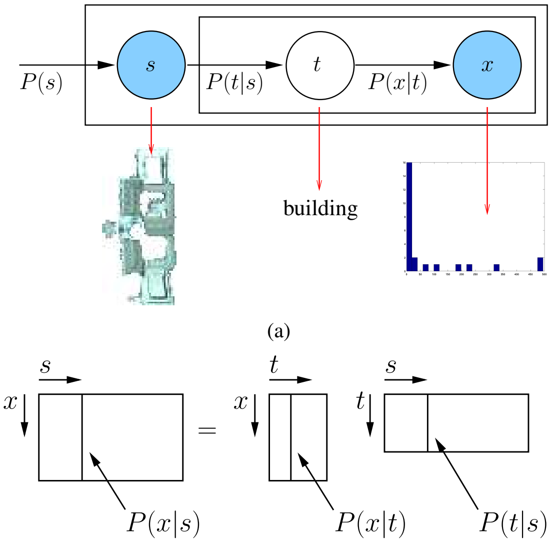

(a)

(b)

Fig. 15. (a) PLSA graphical model. The filled nodes indicate observed random variables whereas the unfilled node is unobserved. The red arrows show examples for the measurements represented at each node. (b) In PLSA, the object specific feature probability, $P(x_j|t_k)$, and the segment specific object probability, $P(t_k|s_i)$, are used to compute the segment specific feature probability, $P(x_j|s_i)$.

the posterior probability of the latent variables are computed based on the current estimates of the parameters as

$$P(t_k|s_i, x_j) = \frac{P(x_j|t_k)P(t_k|s_i)}{\sum_{l=1}^{K} P(x_j|t_l)P(t_l|s_i)}. \quad (3)$$

In the M-step, the parameters are updated to maximize the expected complete data log-likelihood as

$$P(x_j|t_k) = \frac{\sum_{i=1}^{N} n(s_i, x_j)P(t_k|s_i, x_j)}{\sum_{m=1}^{M} \sum_{i=1}^{N} n(s_i, x_m)P(t_k|s_i, x_m)}, \quad (4)$$

$$P(t_k|s_i) = \frac{\sum_{j=1}^{M} n(s_i, x_j)P(t_k|s_i, x_j)}{\sum_{j=1}^{M} n(s_i, x_j)}. \quad (5)$$

The E-step and the M-step are iterated until the difference between the consecutive expected complete data log-likelihoods is less than a threshold or the number of iterations exceeds a predetermined value.

C. Detecting Objects

After learning the parameters of the model, we want to find good segments belonging to each learned object type. This is done by comparing the feature distribution within each segment, $p(x|s)$, and the feature distribution for a given object type, $p(x|t)$. The similarity between two distributions can be measured using the Kullback-Leibler (KL) divergence $D(p(x|s)\|p(x|t))$. Then, for each object type, the segments in an image can be sorted according to their KL divergence scores, and the most representative segments for that object type can be selected. However, if there are two segments that are extracted from different spectral bands grouped within the same object type and at least one of them overlaps with the other by a predetermined percent of its whole area, the less representative structure (the one with a larger KL divergence score) is removed from that object type to avoid having multiple segments of the same object.

D. Evaluation of Object Detection

The performance of the PLSA-based segment grouping and object detection depends on the choice of the features that are used to model the segments and the number of object types that is given as input to the grouping algorithm. Clustering evaluation measures can be used to study the effects of different settings of the parameters and provide an objective and quantitative evaluation of the unsupervised grouping/detection algorithms described in the previous sections.

In the literature, clustering is often used as an intermediate step of a classification/recognition system where only the performance of the final system is analyzed, or usually only a qualitative visual inspection of the clustering results are performed. To evaluate the accuracy of object detection, first, quality measures for both individual object types (clusters) and the overall detection (clustering) must be defined. One way of defining these measures involves the use of ground truth data where the resulting groups are compared to the manually assigned labels for the segments. In other words, the quality measures should quantify how well the results of the unsupervised detection algorithm reflect the groupings in the ground truth.

In an optimal result, the segments with the same object class labels in the ground truth must be assigned to the same group (cluster) and the segments corresponding to different object class types must appear in different groups (clusters) at the end of the detection process. An information theoretic criterion that measures the homogeneity of the distribution of the segments with respect to different object types is the entropy [22]. Another measure is the Rand index [23] that is analogous to the Kappa coefficient and measures the agreement between two labellings. These two measures are described below.

1) Entropy: Let h_{ck} denote the number of segments assigned to the object type (cluster) k with a ground truth object class label c, $h_{c.} = \sum_{k=1}^{K} h_{ck}$ denote the number of segments with a ground truth object class label c, and $h_{.k} = \sum_{c=1}^{C} h_{ck}$ denote the number of segments assigned to object type (cluster) k, where K is the number of object types given as input to the grouping/detection algorithm and C is the true number of objects. The quality of individual clusters is measured in terms of the homogeneity of the true object class labels within each cluster. For each cluster k, the cluster entropy E_k is given by

$$E_k = -\sum_{c=1}^{C} \frac{h_{ck}}{h_{.k}} \log \frac{h_{ck}}{h_{.k}}. \quad (6)$$

Then, the overall cluster entropy E_{cluster} is given by a weighted sum of individual cluster entropies as

$$E_{\text{cluster}} = \frac{1}{\sum_{k=1}^{K} h_{.k}} \sum_{k=1}^{K} h_{.k} E_k. \quad (7)$$

A smaller cluster entropy value indicates a higher homogeneity. However, the cluster entropy continues to decrease as the number of clusters increases. To overcome this problem, another entropy criterion that measures how segments of the same true object class are distributed among the clusters can be defined. For each true object class c, the class entropy E_c is given by

$$E_c = -\sum_{k=1}^{K} \frac{h_{ck}}{h_{c.}} \log \frac{h_{ck}}{h_{c.}}. \tag{8}$$

Then, the overall class entropy E_{class} is given by a weighted sum of individual class entropies as

$$E_{\text{class}} = \frac{1}{\sum_{c=1}^{C} h_{c.}} \sum_{c=1}^{C} h_{c.} E_c. \tag{9}$$

Unlike the cluster entropy, the class entropy increases when the number of clusters increase. Therefore, the two measures can be combined for an overall entropy measure as

$$E = \beta E_{\text{cluster}} + (1 - \beta) E_{\text{class}} \tag{10}$$

where $\beta \in [0, 1]$ is a weight that balances the two measures [22].

2) Adjusted Rand index: When the number of true object classes and the number of detected object types are the same, the Kappa coefficient can be used to measure the amount of agreement between the two labellings. However, the number of detected clusters in unsupervised classification is not always the same as the true number of objects. In such cases, the Rand index can be used to measure the agreement of every pair of segments according to both unsupervised and ground truth labellings [23]. The agreement occurs if two segments that belong to the same class are put into the same cluster, or two segments that belong to different classes are put into different clusters. The Rand index is computed as the proportion of all segment pairs that agree in their labels. The index has a value between 0 and 1, where 0 indicates that the two labellings do not agree on any pair of segments and 1 indicates that the two labellings are exactly the same.

However, the expected value of the Rand index of two random groupings does not take a constant value. The adjusted Rand index [23], which can be computed as

$$R = \frac{\sum_{c=1}^{C}\sum_{k=1}^{K}\binom{h_{ck}}{2} - \left[\sum_{c=1}^{C}\binom{h_{c.}}{2}\sum_{k=1}^{K}\binom{h_{.k}}{2}\right] / \binom{N}{2}}{\left[\sum_{c=1}^{C}\binom{h_{c.}}{2} + \sum_{k=1}^{K}\binom{h_{.k}}{2}\right] / 2 - \left[\sum_{c=1}^{C}\binom{h_{c.}}{2}\sum_{k=1}^{K}\binom{h_{.k}}{2}\right] / \binom{N}{2}} \tag{11}$$

where N is the total number of segments, has a maximum value of 1 and an expected value of 0. Therefore, it has a wider range and more sensitivity than the original index. This index is also analogous to the Kappa coefficient because it measures the agreement over and above that expected by chance [23].

3) Ground truth for object detection: Since suitable detailed GIS data and object level ground truth are not available in the form of individual segments, we use the pixel level ground truth to generate the object labels for evaluation. The pixel level ground truth that we manually created and is shown in Figure 16(a) is used for this purpose. Given all segments that are used for object detection, a segment is assigned an object class label if at least 20% of its pixels have an overlap with the pixel level ground truth and at least 50% of those pixels have the same label. The first threshold handles the areas where the pixel level ground truth is not available. The second threshold ensures that the majority of the segment belongs to the same object. These two thresholds are selected empirically to obtain an object level ground truth with a coverage as much as possible by making use of the pixel level ground truth as much as possible. These object labels for segments are used to perform a quantitative evaluation of the unsupervised object detection.

V. Experiments

Qualitative evaluation of the proposed image segmentation algorithm with comparative experiments was presented in Section III-D. The input to the unsupervised object detection algorithm is the set of all segments extracted from individual bands of an image where the goal is to find coherent groups of segments that correspond to different objects. The total number of segments automatically extracted was 2,070, 4,107 and 1,053 for the *DC Mall*, *Pavia* and *Ankara* data sets, respectively.

The next step is the modeling of the segments using histograms of quantized feature values. All seven possible combinations of three different types of features (PCA, LDA, Gabor) for the *DC Mall* and *Pavia* data sets, and three possible combinations of two different types of features (RGB, Gabor) for the *Ankara* data set were used as described in Section II. The pixels in each image were quantized using the k-means algorithm where the number of quantization levels (k) was set to three different values (10, 25, 40) to study the effects of quantization. Then, for each segment, a histogram with k bins was constructed by counting the number of pixels belonging to each quantization level within that segment as described in Section IV-A.

Next, the PLSA algorithm was used to learn the object-conditional feature distributions for all object types. In the experiments, the number (K) of latent object type variables (t_k) was varied from 5 to 60 with increments of 1. The parameters of the distribution models were learned using the EM algorithm for each setting as described in Section IV-B.

In the final step, the KL divergence score between each segment and each object type was computed, and the segments were grouped as belonging to the object type where the KL score was the smallest. Since the segments were extracted from different bands, some of the segments could overlap. When the overlap between two segments belonging to the same group was more than 30% of the area of one of the segments, the one with a larger KL divergence score was removed as described in Section IV-C.

Quantitative performance evaluation for object detection was performed for the *DC Mall* data set using the performance indices described in Section IV-D. We extended the original pixel level ground truth containing only 8,079 pixels that we obtained with the hyper-spectral data [24] to increase its coverage as much as possible (shown in Figure 16(a)). Figure 16 shows the entropy and Rand indices with respect to different settings of the features, the number of quantization levels, and the number of object types (number of clusters). When individual cluster entropy and class entropy values are analyzed in detail, we can see that the cluster entropy continued to decrease as expected as the number of clusters increased because purer clusters were obtained when the segments were divided into a larger number of groups. On the other hand, the class entropy tended to stay flat for very small number of clusters and started to increase when the number of clusters became greater than the number of true object classes ($C = 7$ for this data set) because the segments belonging to the same object class were divided into more and more groups, diversifying the distribution of the class over the clusters. The turning point for the overall entropy occurred when the number of clusters was approximately equal to the number of true object classes (around $K = 8$ or 9), after which it continued to increase because the increase in the class entropy was greater than the decrease in the cluster entropy.

The Rand index measures the agreement between the detected and true segment labels using two components: the number of segment pairs that belong to the same class and put into the same cluster, and the number of segment pairs that belong to different classes and put into different clusters. In the experiments, the former number tended to stay flat for very small number of clusters and started to decrease as expected when the number of clusters became greater than the number of true object classes because the segments of the same object type were divided into different clusters. On the other hand, the latter number continued to increase as expected as the number of clusters increased. The overall Rand index followed the former number because its decrease was more significant than the increase in the latter. Note that, the adjusted Rand index values above 30% correspond to an agreement of above 80% between the detected and ground truth labels of every pair of segments according to the definition of the original Rand index in [23].

When the effects of different feature combinations are analyzed, we can see that individually LDA features performed better than PCA and Gabor features. This is expected because pixel level class labels are used to extract these features so that they maximize class separability whereas the PCA and Gabor features are computed using unsupervised techniques. The feature combinations that include LDA features also performed better than other combinations for the same reasons. Gabor features were not as effective as others because such features are generally useful for large textured areas such as vegetation but many building segments did not gain additional information from texture because their support (area) were usually too small compared to the sizes of the texture filters. When PCA (spectral) features are compared to LDA features, the latter were very effective in distributing segments that belong to different object classes such as buildings, vegetation, roads, etc. to different groups (clusters) whereas the former were powerful in distinguishing buildings with different types of roofs (all buildings were in the same ground truth class called roof). Therefore, they provide complementary information and usually the best results were obtained when they were used together but the results with only PCA features were also acceptable and show that the grouping technique is very powerful for unsupervised object detection even when no manual label information is available.

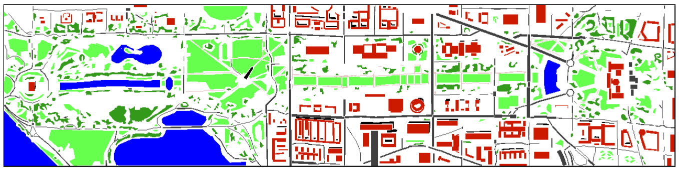

(a) Reference map (rotated)

Class	Roof	Street	Path	Grass	Trees	Water	Shadow	Total
	🟥	⬛	🟫	🟩	🟩	🟦	⬛	
Pixel level	28975	19175	2027	43399	18406	25491	2160	139633
Object level	154	169	45	175	256	7	44	850

(b) Ground truth statistics (number of pixels and segments in each class)

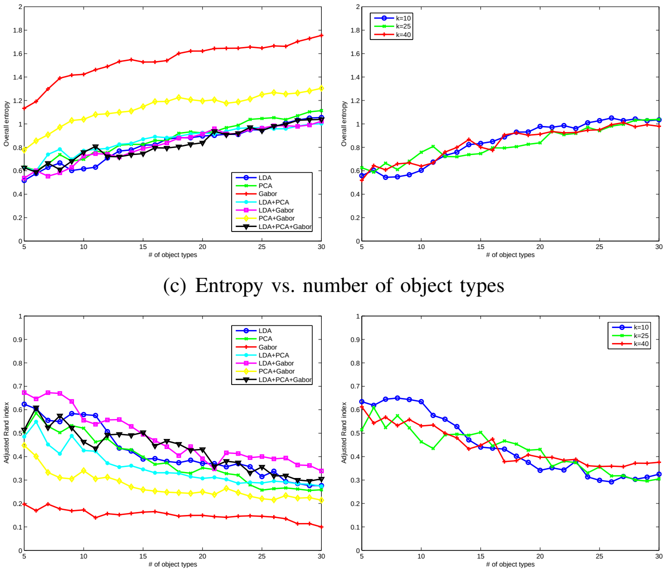

(c) Entropy vs. number of object types

(d) Adjusted Rand index vs. number of object types

Fig. 16. The reference map and the statistics of the ground truth used to compute the object detection performance indices. The plots in (c) and (d) show the indices for different settings of the features for $k = 25$ (left) and for different number of quantization levels ($k = 10, 25, 40$) when PCA, LDA and Gabor features were used (right). The x-axes show the number of object types (K, number of clusters) given as input to the detection algorithm.

When the effect of the number of quantization levels is analyzed, we did not observe any significant difference between $k = 10$, 25 or 40. Finally, even though there were some differences in the performance index values for different feature combinations, visual inspection of the resulting groups showed that these differences occurred mostly because of different groupings of the small tree and grass segments. Even though the major and relatively larger segments such as buildings or roads were grouped similarly with different feature combinations, there were some differences in the grouping of small vegetation segments (especially when K was increased) that were larger in number compared to other object types, and this caused some differences in the performance indices.

Note that, the quantitative performance indices actually provide a “pessimistic” estimate of the actual performance because, for example, two different kinds of buildings with different roof types that are correctly put into different clusters by the object detection algorithm will decrease the Rand

TABLE II
THE NUMBER OF AUTOMATICALLY DETECTED SEGMENTS FOR ROADS, BUILDINGS AND VEGETATION OBJECTS, AND THE CORRESPONDING PRECISION AND RECALL VALUES (AS PERCENTAGES) FOR DIFFERENT NUMBER OF CLUSTERS (K).

	Roads			Buildings			Vegetation		
K	Detect	Prec	Recall	Detect	Prec	Recall	Detect	Prec	Recall
5	498	33.53	86.98	240	75.42	75.32	945	56.19	93.90
15	428	35.98	86.39	295	67.80	75.32	874	59.04	92.49
25	326	46.63	80.47	325	66.15	85.71	945	55.98	93.19

index if those two visually different buildings have the same ground truth label as "roof". Even though the ground truth may not contain that much detail, visual evaluation confirms that such cases can be correctly handled by our algorithm. This also shows that there may not be a single best value for K but one can interpret the plots like in Figure 16 by looking at the significant changes in the performance indices that occur when a significant new cluster (group) is produced when the number of object types is increased. Therefore, a natural extension of this unsupervised grouping process is the selection and labeling of the detected groups by the user for a final classification with a desired level of detail.

In addition to the entropy and Rand indices, we also evaluated the performance of the proposed object detection algorithm using precision and recall to measure how well the detected objects correspond to the ground truth objects. Given the segment groups (clusters) obtained using the unsupervised detection algorithm for a specific value of K, first, we manually identified the groups containing roads, buildings and vegetation according to the content of the majority of the segments using visual inspection. For a segment to be accepted as a correct detection, it must have a sufficient overlap with an object in the ground truth. Then, we used the object level ground truth described in Section IV-D, and for each object type, computed precision and recall as:

$$\text{precision} = \frac{\text{\# of correctly detected objects (segments)}}{\text{\# of all detected objects (segments)}}, \quad (12)$$

$$\text{recall} = \frac{\text{\# of correctly detected objects (segments)}}{\text{\# of all objects in the ground truth}}. \quad (13)$$

Recall can be interpreted as the number of true positive objects extracted by the algorithm, while precision evaluates the tendency of the algorithm for false positives [17]. The results for three different values of K are shown in Table II. We believe that the results are quite satisfactory given the complexity of the data and the unsupervised nature of the algorithm used.

Figure 17 shows example groups obtained for the *DC Mall* data set when PCA, LDA and Gabor features were used with 25 quantization levels. The clusters for $K = 5$ contained roads/shadow, buildings/water, buildings/soil, trees/grass, grass, and were already quite meaningful for a small K. When K was increased, trees and grass segments started separating further. At $K = 8$, the water segments separated from buildings.[1] At $K = 10$, the building segments started separating into different clusters according to their roof types. Further increase in K caused grass segments to be divided into more clusters (e.g., greener segments vs. browner segments). At $K = 17$, most of the shadow segments separated from roads. Larger values of K produced small clusters that contained small tree or grass segments because there were more such segments compared to segments of other types.

Similarly, Figures 18 and 19 show example results for *Pavia* and *Ankara* data sets, respectively. Due to space limitations, instead of individual clusters, the segments belonging to the groups that mostly contain buildings, roads, and vegetation are shown. For the *Pavia* image, all buildings with tile roofs were grouped together with almost no false alarms. There were some minor confusions between the roads and some shadow segments and buildings with very similar colors. For the *Ankara* image, the clusters were almost complete when $K = 5$. Overall, the quantitative evaluation using performance indices and the qualitative visual inspection of the detection results for all data sets confirmed that the proposed algorithms were able to identify the segments corresponding to objects (i.e., "good" segments) by placing them into coherent groups in an unsupervised mode, where there is a strong correlation between the true object labels and the detected segment labels.

VI. CONCLUSIONS

We presented novel methods for unsupervised image segmentation and automatic object detection in high-resolution remotely sensed imagery. Our segmentation algorithm exploited structural information using morphological operators. These operators were applied to each spectral band separately where candidate segments were extracted by applying connected components analysis to the pixels selected according to their morphological profiles. These segments were modeled hierarchically using a tree, and the most meaningful ones in this hierarchy were selected by optimizing a criterion that consisted of two factors: spectral homogeneity and neighborhood connectivity. The segment selection algorithm is generic in the sense that not only can other criteria for a "good" (meaningful) segment be directly incorporated, but it can also be used with other hierarchical segmentation algorithms.

We evaluated the proposed approach qualitatively on three data sets. The results showed that our method that considers morphological characteristics, spectral information, and their consistency within neighboring pixels is able to detect structures in the image which are more precise and more meaningful than the structures detected by two popular approaches that do not make strong use of neighborhood and spectral information jointly.

We also proposed an object detection algorithm that formulated the detection process as an unsupervised grouping

[1] Some large water segments do not appear in the results because small structuring elements (maximum radius of 15) were used in the morphological profile as we are mainly interested in smaller structures such as buildings. All water segments can be extracted using larger structuring elements. Alternatively, simple thresholding of spectral bands can detect water segments before running our object detection algorithm.

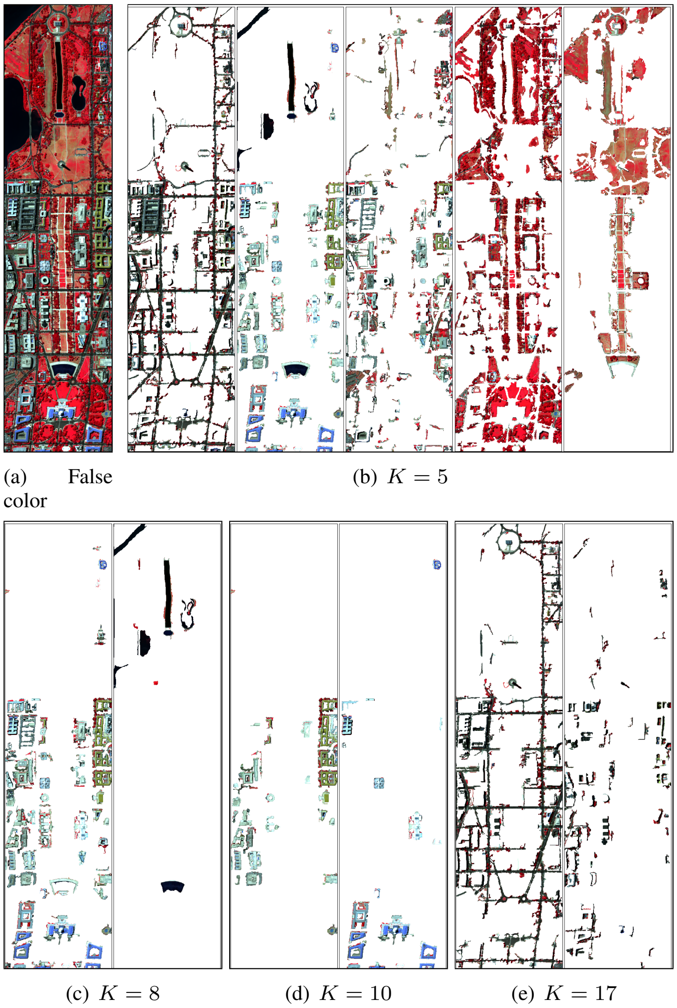

(a) False color (b) $K = 5$

(c) $K = 8$ (d) $K = 10$ (e) $K = 17$

Fig. 17. Examples of object detection for the *DC Mall* data set. (b) Clusters when $K = 5$. The groupings are already meaningful for a small K. (c) Two new clusters introduced when $K = 8$. The second cluster in (b) is divided into building and water segments. (d) Two new clusters introduced when $K = 10$. The building segments in the first cluster in (c) are further divided according to their roof types. (e) Two new clusters introduced when $K = 17$. The first cluster in (b) is divided into road and shadow segments.

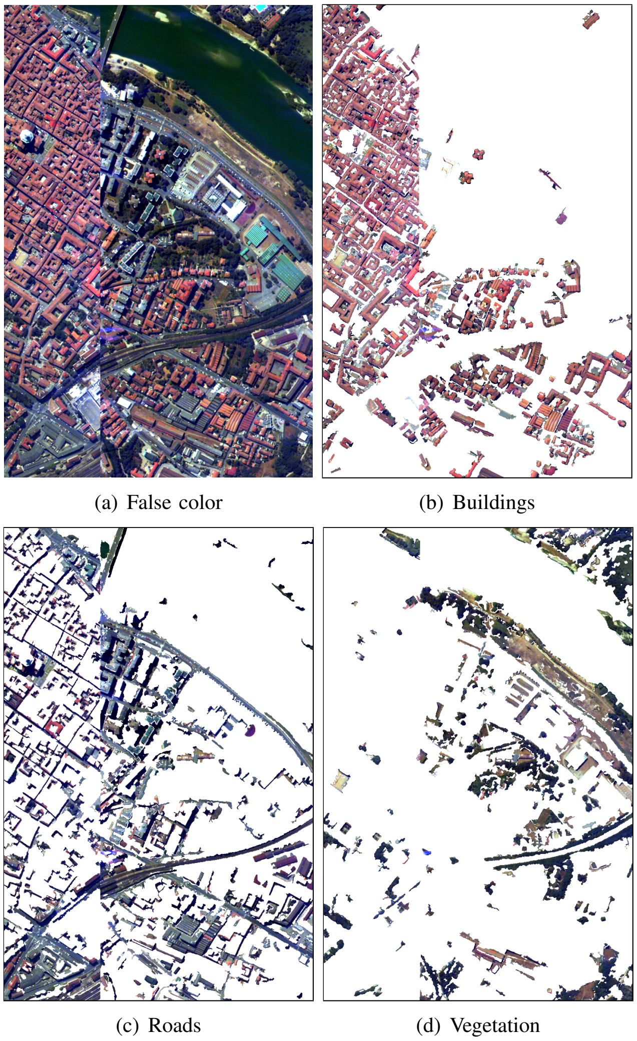

(a) False color (b) Buildings

(c) Roads (d) Vegetation

Fig. 18. Examples of object detection for the *Pavia* data set when $K = 30$.

problem for automatic selection of coherent sets of segments corresponding to meaningful structures among a set of candidate segments from multiple hierarchical segmentations obtained from individual spectral bands. The grouping problem was solved using the probabilistic Latent Semantic Analysis algorithm that built object models by learning the object-conditional feature probability distributions. Automatic labeling of a segment was done by comparing its spectral and textural content distribution to the distribution of the learned object models. The object detection algorithm is generic in the sense that any model for a segment's content can be used by the grouping algorithm. Extensive performance evaluation showed that the proposed methods are able to automatically detect and group structures belonging to the same object classes.

Acknowledgment

The authors thank Dr. David A. Landgrebe and Mr. Larry L. Biehl from Purdue University, U.S.A., for the *DC Mall* data set, Dr. Paolo Gamba from the University of Pavia, Italy, for the *Pavia* data set, and the Scientific and Technological Research Council of Turkey (TUBITAK) for the *Ankara* data set.

References

[1] S. Aksoy, "Spatial techniques for image classification," in *Signal and Image Processing for Remote Sensing*, C. H. Chen, Ed. Taylor & Francis Books, 2006, pp. 489–511.

[2] J. A. Benediktsson, J. A. Palmason, and J. R. Sveinsson, "Classification of hyperspectral data from urban areas based on extended morphological profiles," *IEEE Transactions on Geoscience and Remote Sensing*, vol. 43, no. 3, pp. 480–491, March 2005.

[3] S. Bhagavathy and B. S. Manjunath, "Modeling and detection of geospatial objects using texture motifs," *IEEE Transactions on Geoscience and Remote Sensing*, vol. 44, no. 12, pp. 3706–3715, December 2006.

[4] M. Pesaresi and J. A. Benediktsson, "A new approach for the morphological segmentation of high-resolution satellite imagery," *IEEE Transactions on Geoscience and Remote Sensing*, vol. 39, no. 2, pp. 309–320, February 2001.

[5] F. Melgani and S. B. Serpico, "A Markov random field approach to spatio-temporal contextual image classification," *IEEE Transactions on Geoscience and Remote Sensing*, vol. 41, no. 11, pp. 2478–2487, November 2003.

[6] L. Bruzzone and L. Carlin, "A multilevel context-based system for classification of very high spatial resolution images," *IEEE Transactions*

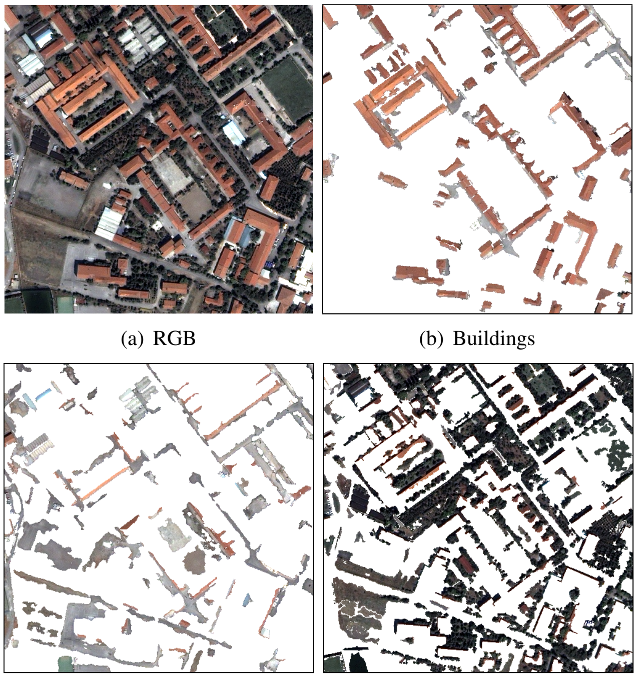

(a) RGB

(b) Buildings

(c) Roads

(d) Vegetation

Fig. 19. Examples of object detection for the *Ankara* data set when $K = 5$.

on Geoscience and Remote Sensing, vol. 44, no. 9, pp. 2587–2600, September 2006.

[7] S. Aksoy and H. G. Akcay, "Multi-resolution segmentation and shape analysis for remote sensing image classification," in *Proceedings of 2nd International Conference on Recent Advances in Space Technologies*, Istanbul, Turkey, June 9–11, 2005, pp. 599–604.

[8] A. Katartzis, I. Vanhamel, and H. Sahli, "A hierarchical markovian model for multiscale region-based classification of vector-valued images," *IEEE Transactions on Geoscience and Remote Sensing*, vol. 43, no. 3, pp. 548–558, March 2005.

[9] L. K. Soh, C. Tsatsoulis, D. Gineris, and C. Bertoia, "ARKTOS: an intelligent system for sar sea ice image classification," *IEEE Transactions on Geoscience and Remote Sensing*, vol. 2, no. 1, pp. 229–248, January 2004.

[10] S. Aksoy, K. Koperski, C. Tusk, G. Marchisio, and J. C. Tilton, "Learning Bayesian classifiers for scene classification with a visual grammar," *IEEE Transactions on Geoscience and Remote Sensing*, vol. 43, no. 3, pp. 581–589, March 2005.

[11] J. C. Tilton, "Analysis of hierarchically related image segmentations," in *Proceedings of IEEE GRSS Workshop on Advances in Techniques for Analysis of Remotely Sensed Data*, Washington, DC, October 27–28, 2003, pp. 60–69.

[12] A. Darwish, K. Leukert, and W. Reinhardt, "Image segmentation for the purpose of object-based classification," in *Proceedings of IEEE International Geoscience and Remote Sensing Symposium*, vol. 3, Toulouse, France, July 21–25, 2003, pp. 2039–2041.

[13] T. Hofmann, "Unsupervised learning by probabilistic latent semantic analysis," *Machine Learning*, vol. 42, no. 1–2, pp. 177–196, January–February 2001.

[14] R. O. Duda, P. E. Hart, and D. G. Stork, *Pattern Classification*. John Wiley & Sons, Inc., 2000.

[15] H. G. Akcay and S. Aksoy, "Morphological segmentation of urban structures," in *Proceedings of 4th IEEE GRSS/ISPRS Joint Workshop on Remote Sensing and Data Fusion over Urban Areas*, Paris, France, April 11–13, 2007.

[16] A. J. Plaza and J. C. Tilton, "Automated selection of results in hierarchical segmentations of remotely sensed hyperspectral images," in *Proceedings of IEEE International Geoscience and Remote Sensing Symposium*, vol. 7, Seoul, Korea, July 25–29, 2005, pp. 4946–4949.

[17] M. Klaric, G. Scott, C.-R. Shyu, and C. Davis, "Automated object extraction through simplification of the differential morphological profile for high-resolution satellite imagery," in *Proceedings of IEEE International Geoscience and Remote Sensing Symposium*, vol. 2, Seoul, Korea, July 25–29, 2005, pp. 1265–1268.

[18] G. Hamerly and C. Elkan, "Learning the k in k-means," in *Neural Information Processing Systems*, Vancouver, Canada, December 8–13, 2003, pp. 281–288.

[19] P. Soille, *Morphological Image Analysis*, 2nd ed. Springer, 2002.

[20] H. G. Akcay and S. Aksoy, "Automated detection of objects using multiple hierarchical segmentations," in *Proceedings of IEEE International Geoscience and Remote Sensing Symposium*, Barcelona, Spain, July 23–27, 2007.

[21] B. C. Russell, A. A. Efros, J. Sivic, W. T. Freeman, and A. Zisserman, "Using multiple segmentations to discover objects and their extent in image collections," in *Proceedings of IEEE Conference on Computer Vision and Pattern Recognition*, vol. 2, New York, NY, June 17–22, 2006, pp. 1605–1614.

[22] J. He, A.-H. Tan, C.-L. Tan, and S.-Y. Sung, "On quantitative evaluation of clustering systems," in *Information Retrieval and Clustering*, W. Wu, H. Xiong, and S. Shekhar, Eds. Kluwer Academic Publishers, 2003.

[23] B. S. Everitt, S. Landau, and M. Leese, *Cluster Analysis*, 4th ed. Oxford University Press, 2001.

[24] D. A. Landgrebe, *Signal Theory Methods in Multispectral Remote Sensing*. John Wiley & Sons, Inc., 2003.

H. Gökhan Akçay received the B.S. and M.S. degrees in computer engineering from Bilkent University, Ankara, Turkey, in 2004 and 2007, respectively. He is currently pursuing the Ph.D. degree in computer engineering at Bilkent University.

Since September 2004, he has been a Teaching and Research Assistant at the Department of Computer Engineering, Bilkent University. His research interests include statistical and structural pattern recognition, computer vision and remote sensing image analysis.

Selim Aksoy (S'96-M'01) received the B.S. degree from the Middle East Technical University, Ankara, Turkey, in 1996 and the M.S. and Ph.D. degrees from the University of Washington, Seattle, in 1998 and 2001, respectively.

He has been an Assistant Professor at the Department of Computer Engineering, Bilkent University, Ankara, since 2004, where he is also the Co-Director of the RETINA Vision and Learning Group. Before joining Bilkent, he was a Research Scientist at Insightful Corporation, Seattle, where he was involved in image understanding and data mining research sponsored by the National Aeronautics and Space Administration, the U.S. Army, and the National Institutes of Health. During 1996–2001, he was a Research Assistant at the University of Washington, where he developed algorithms for content-based image retrieval, statistical pattern recognition, object recognition, graph-theoretic clustering, user relevance feedback, and mathematical morphology. During the summers of 1998 and 1999, he was a Visiting Researcher at the Tampere International Center for Signal Processing, Tampere, Finland, collaborating in a content-based multimedia retrieval project. His research interests include computer vision, statistical and structural pattern recognition, machine learning and data mining with applications to remote sensing, medical imaging, and multimedia data analysis.

Dr. Aksoy is a member of the IEEE Geoscience and Remote Sensing Society, the IEEE Computer Society, and the International Association for Pattern Recognition (IAPR). His received the CAREER Award from the Scientific and Technological Research Council of Turkey (TUBITAK) in 2004. He was one of the Guest Editors of the special issue of IEEE Transactions on Geoscience and Remote Sensing on Pattern Recognition in Remote Sensing in 2007. He served as the Vice Chair of the IAPR Technical Committee 7 on Remote Sensing during 2004–2006 and is currently the Chair of the same committee for 2006–2008.